Electrically driven phase transition in magnetite nanostructures

SUNGBAE LEE[1], ALEXANDRA FURSINA[2], JOHN T. MAYO[2], CAFER T. YAVUZ[2], VICKI L. COLVIN[2], R. G. SUMESH SOFIN[3], IGOR V. SHVETS[3] AND DOUGLAS NATELSON[1,4]*

[1]Department of Physics and Astronomy, Rice University, 6100 Main St., Houston, Texas 77005, USA
[2]Department of Chemistry, Rice University, 6100 Main St., Houston, Texas 77005, USA
[3]CRANN, School of Physics, Trinity College, Dublin 2, Ireland
[4]Department of Electrical and Computer Engineering, Rice University, 6100 Main St., Houston, Texas 77005, USA
*e-mail: natelson@rice.edu

Published online: 16 December 2007; doi:10.1038/nmat2084

Magnetite (Fe_3O_4), an archetypal transition-metal oxide, has been used for thousands of years, from lodestones in primitive compasses[1] to a candidate material for magnetoelectronic devices[2]. In 1939, Verwey[3] found that bulk magnetite undergoes a transition at $T_V \approx 120$ K from a high-temperature 'bad metal' conducting phase to a low-temperature insulating phase. He suggested[4] that high-temperature conduction is through the fluctuating and correlated valences of the octahedral iron atoms, and that the transition is the onset of charge ordering on cooling. The Verwey transition mechanism and the question of charge ordering remain highly controversial[5–11]. Here, we show that magnetite nanocrystals and single-crystal thin films exhibit an electrically driven phase transition below the Verwey temperature. The signature of this transition is the onset of sharp conductance switching in high electric fields, hysteretic in voltage. We demonstrate that this transition is not due to local heating, but instead is due to the breakdown of the correlated insulating state when driven out of equilibrium by electrical bias. We anticipate that further studies of this newly observed transition and its low-temperature conducting phase will shed light on how charge ordering and vibrational degrees of freedom determine the ground state of this important compound.

Strongly correlated electronic materials can exhibit pronounced electronic properties (for example, high-temperature superconductivity, metal–insulator transitions and charge ordering) not present in simple systems with weaker electron–electron interactions. Such rich electronic phenomenology can result when electron–electron interactions, electron–phonon interactions and electronic bandwidth are all of similar magnitude, as in magnetite[12]. Verwey[3] found nearly seven decades ago that bulk magnetite, although moderately conductive at room temperature, undergoes a transition to a more insulating state below what is now called the Verwey temperature, $T_V \approx 120$ K. Similar transitions are known in a number of materials[13,14]. Above T_V, Fe_3O_4 has an inverse-spinel structure of the form AB_2O_4, with tetrahedrally coordinated A sites occupied by Fe^{3+} and octrahedrally coordinated B sites of mixed valence, equally occupied by iron atoms with formal +3 and +2 charges. Conduction at high temperatures has long been thought to be through fluctuating valences of the B sites, with the transition corresponding to some kind of B-site charge ordering as T decreases; concurrent is a first-order structural phase transition to a monoclinic unit cell. This explanation remains controversial[5,6], with experiments showing some charge disproportion or charge order[7,8], and others implying that the structural degrees of freedom drive the change in conductivity[9,10]. Recent theoretical progress has been made in understanding the complex interplay of charge and structural degrees of freedom[15,16], including a complete picture of the transition mechanism[11] with strongly correlated $3d$ Fe electrons acting to amplify electron–phonon couplings. Testing these ideas experimentally is of much interest.

Here, we report electronic transport measurements in magnetite at the nanoscale on both nanocrystals and single-crystal epitaxial thin films. Both types of device exhibit pronounced electrically driven hysteretic switching of the electronic conductance once sample temperatures are reduced below T_V. The data clearly show that the transition is not the result of local heating above T_V, but instead is an electrically driven breakdown of the insulating state. We discuss possible explanations for this switching in the context of the general Verwey transition problem. Whereas qualitatively similar resistive switching has been observed in other correlated oxide systems[17,18], the phenomenon in Fe_3O_4 is a bulk effect with a mechanism distinct from these.

Two-terminal devices for applying voltages and measuring conduction at the nanoscale have been fabricated (see the Methods section) incorporating both Fe_3O_4 nanocrystals[19] (10–20 nm in diameter with oleic acid coating) and single-crystal thin films (40–60 nm thick)[20]. Devices were measured in both a variable-temperature vacuum probe station and a ^{4}He cryostat with a magnet. Current–voltage characteristics have been measured with both a semiconductor parameter analyser and directly using voltage sources and current amplifiers, with differential conductance computed numerically.

Figure 1a shows I–V characteristics of a nanocrystal device at selected temperatures. When cooling, zero-bias conductance decreases monotonically until $T \to T_V$. Below T_V, the I–V characteristics show sharp switching between a low-bias insulating state and a high-bias state with much higher differential conductance $dI/dV(V)$ (close to $dI/dV(V=0, T=300\,\mathrm{K})$), with pronounced hysteresis as a function of voltage sweep direction. The switching threshold voltages increase in magnitude as T is decreased.

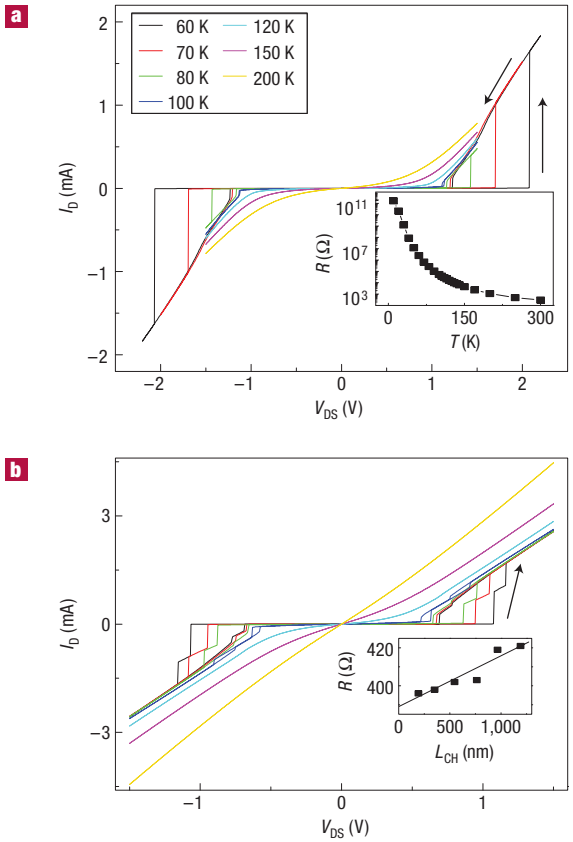

Figure 1 Hysteretic conductance switching below T_V. a, Current–voltage characteristics at various temperatures for a device based on 10 nm magnetite nanocrystals. Arrows indicate the direction of the hysteresis. Inset: Zero-bias resistance, $R(T)$. **b**, Analogous data for a device based on a 50-nm-thick magnetite film grown by molecular beam epitaxy. The nominal interelectrode gap was planned to be 100 nm, but at its narrowest was approximately 10 nm. Inset: Two-terminal resistance as a function of channel length for another set of devices fabricated on another piece of the same film, at 300 K.

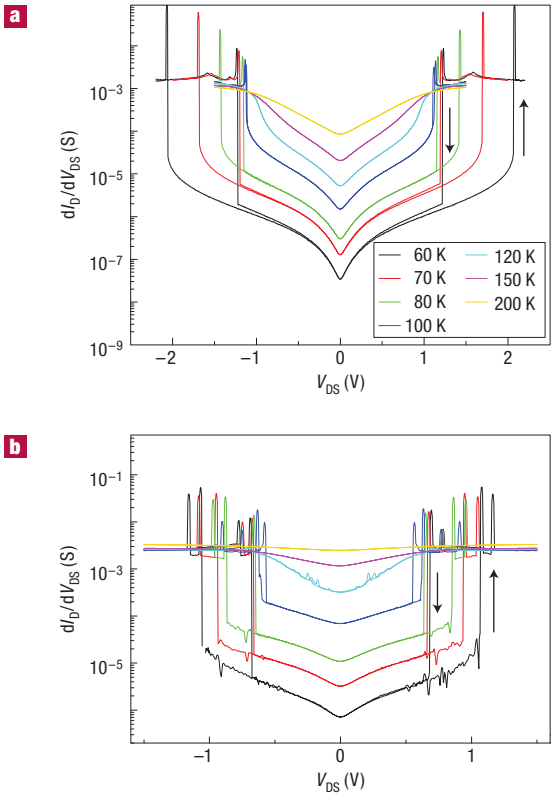

Figure 2 Differential conductance plots of the switching. a, dI/dV versus V for the nanocrystal device from Fig. 1a at the same temperatures. **b**, dI/dV versus V for the thin-film device from Fig. 1b. Both plots have logarithmic dI/dV axes to better show the lowest temperature data.

Dozens of nanocrystal devices were measured and only those with 300 K resistances below 10 kΩ showed the switching, with higher resistance devices having higher switching threshold voltages. Resistances decrease by three orders of magnitude with vacuum annealing at 673 K, probably because of oleic acid decomposition[21,22]. The temperature dependence (Fig. 1a, inset) of the zero-bias resistance, $R(T)$, has no step at T_V, showing that $R(T)$ remains dominated by contact effects.

Qualitatively identical conduction is apparent in the thin-film devices, as shown in Fig. 1b. Contact resistances are also important in these structures, as demonstrated by examining R at low bias (<100 mV) as a function of channel length, L, as shown in the inset for one set of devices. Extrapolating back to $L \rightarrow 0$, the contact resistance, R_c, at 300 K is 390 Ω, whereas the 50-nm-thick channel of width 20 μm contributes 27.2 Ω μm^{-1}, implying (on the basis of channel geometry) a magnetite resistivity of 2.9 mΩ cm, below bulk expectations. Further investigations are seeking to understand and minimize R_c. Analysis of $R(L)$ at lower temperatures shows that R_c increases significantly as T is decreased, exceeding 80 kΩ by 80 K. This complicates the analysis of the switching, because some of the total V is dropped across R_c rather than directly within the Fe_3O_4; furthermore, the contacts may not be ohmic near the switching threshold. We return to this issue later.

The transitions in all devices are extremely sharp, with widths of less than 50 μV, although in repeated sweeps at a fixed temperature, there is sweep-to-sweep variability of a few millivolts in switching thresholds. Using the substrate as a gate electrode, no discernible gate modulation was seen in nanocrystal devices for gate biases between −80 V and +80 V; this suggests that nanocrystal charging effects do not dominate. Switching characteristics were independent of magnetic field perpendicular to the sample surface up to 9 T, showing no large coupling between magnetization and the transition.

Differential conductance traces (Fig. 2) show the transition even more strikingly. In the high conductance state, dI/dV is relatively temperature independent. As T is decreased, a clear zero-bias suppression develops, deepening into a hard gap when $T < T_V$. In the nanocrystal data there are indications (in $d^2I/dV^2(V)$) of gap formation even at 150 K. We note that T_V in nanocrystals could be elevated, because nanocrystals have large surface-to-volume ratios and the transition temperature of the magnetite surface is known to be higher than in the bulk[23].

Several lines of evidence indicate that these sharp conductance transitions are not the result of local Joule heating (as in macroscopic samples of Fe_3O_4 (refs 24,25) and in the Mott insulator VO_2 (refs 26,27)), but rather are electrically driven. In the worst-case scenario, all of the $I \times V$ Joule heating power is dissipated within the magnetite, and inhomogeneous dissipation (for example, filamentary conduction through a locally heated path) can complicate the analysis. The local steady-state temperature is determined by the power dissipated and the thermal path. Thermally driven switching would then correspond to raising

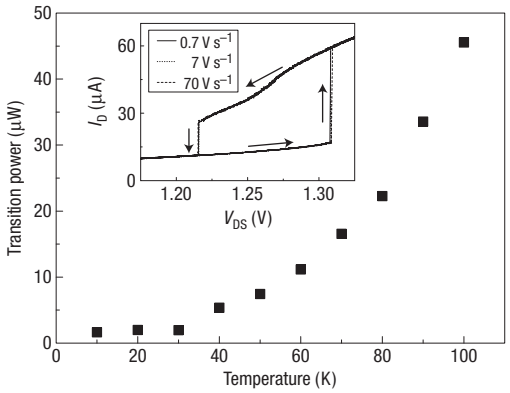

Figure 3 Power required to switch from the insulating into the more conducting state as a function of temperature, for a device based on ~20 nm diameter nanocrystals. Inset: Hysteresis loop in the conduction of the same device at 80 K, showing essentially no change in switching characteristics as the voltage sweep rate is varied over two orders of magnitude.

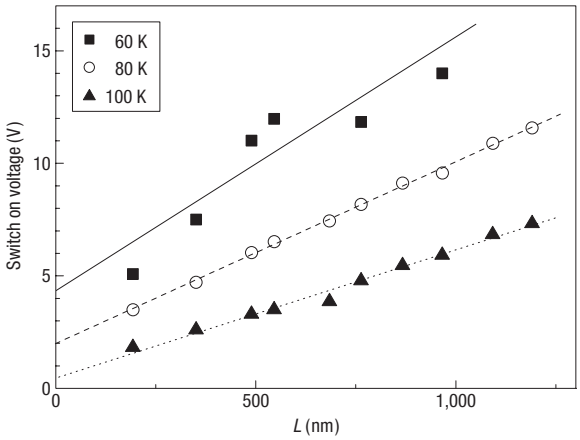

Figure 4 Switching voltages in a series of film devices as a function of channel length at several temperatures. The linear variation with L strongly implies that for each temperature there is a characteristic electric field required for switching. The non-zero intercepts of the trend lines indicate that some device-dependent threshold voltage must be exceeded for switching even when $L = 0$, suggestive of contact effects.

the local temperature above T_V. At a fixed cryostat temperature, an improved thermal path would imply that more power dissipation would be required for a given local temperature rise. Similarly, for a fixed thermal path, the necessary dissipated power for thermal switching would approach zero as $T \rightarrow T_V$. Furthermore, at a given cryostat temperature, thermally driven switching would imply that the power dissipated at the low-to-high conductance transition (needed to raise the local temperature to T_V) should be close to that at the high-to-low conductance transition.

The thermal conductivity, κ, of magnetite is dominated by phonons in this temperature range, and limited by phonon–electron scattering[28], even when $T > T_V$. As a result, κ increases as T is decreased through and below T_V, and the material's thermal coupling to the cryostat improves as T is reduced. In all devices showing switching, the electrical power required to switch from low to high conductance decreases with decreasing T, with Fig. 3 showing one example. This is precisely the opposite of what we would expect from thermally driven switching. Similarly, in all devices the power dissipated at switching does not approach zero as $T \rightarrow T_V$, again inconsistent with thermally driven switching. Furthermore, at a given T the power dissipated just before V is swept back down through the high-to-low conductance threshold significantly exceeds that dissipated at the low-to-high point in many devices, including those in Fig. 1, inconsistent with thermal switching expectations. Finally, nanocrystal and thin-film devices show quantitatively similar switching properties and trends with temperature, despite what would be expected to be very different thermal paths. These switching characteristics are also qualitatively very different from those in known inhomogeneous Joule heating[24,25]. These facts rule out local heating through the Verwey transition as the cause of the conductance switching.

Figure 3 (inset) shows details of hysteresis loops on a nanocrystal device comparing different voltage sweep rates. The loop shape and switching voltages are unchanged to within the precision of the data collection as voltage sweep rates are varied from around 0.7 V s^{-1} up to 70 V s^{-1}. This indicates that the switching process is relatively rapid. Further studies will examine the intrinsic switching speed.

The observed conductance transition seems to be driven electrically. Figure 4 shows a plot of the low-to-high conductance switching voltage as a function of L in a series of film devices for several temperatures. The linear dependence implies that the transition is driven by the electric field itself, rather than by the absolute magnitude of the voltage or the current density. The fact that the voltage extrapolates to a non-zero value at $L = 0$ is probably a contact resistance effect. Minimizing and better understanding the contact resistance will allow the determination of the electric-field distribution within the channel.

The length scaling of the transition voltage also demonstrates that this is a bulk effect. The contacts in all of these devices are identical, so any change in switching properties must result from the magnetite channel. This is in contrast to the resistive switching in $Pr_{0.7}Ca_{0.3}MnO_3$ that is ascribed to a change in contact resistance due to occupation of interfacial states[18].

The field-driven conductance transition may give insights into the equilibrium Verwey transition. This switching may be useful in testing recent calculations[11,15,16] about the role of strongly correlated B-site Fe 3*d* electrons and their coupling to phonons in the Verwey transition mechanism. It is interesting to ask, to what degree is the field-driven electronic transition coupled to the local structure? It is greatly desirable to carry out local probes of the magnetite structure (using X-ray or electron-diffraction techniques or scanned probe microscopy) *in situ* in the channel of biased devices, to see if the coherence between structural symmetry changes and the formation of a gap in the electronic spectrum is broken under these non-equilibrium conditions. This is a significant experimental challenge. Similarly, local Raman spectroscopy of devices under bias could reveal field-induced changes in phonon modes and electron–phonon couplings, and single-crystal thin films permit the application of bias along well-defined crystallographic directions relevant to structural symmetry changes at T_V. We note that qualitatively identical switching occurs in nanocrystal devices as in strained thin films strongly coupled to rigid MgO substrates. This suggests that elastic constraints on scales much larger than the unit cell have relatively little influence on the observed switching.

It is also possible that the non-equilibrium carrier distribution contributes to destabilizing the insulating state. In the presence of a strong electric field, a carrier can gain significant energy even in a single hopping step, even though carrier relaxation times are very short. A rough estimate of the average critical electric field for switching at 80 K is 10^7 V m^{-1}, from the slope of the line in Fig. 4.

The high-temperature cubic unit cell is 0.84 nm on a side, meaning that a carrier traversing one cell would gain approximately 8.4 meV, comparable to $k_B T_V \approx 10.3$ meV. Conductance switching at such high fields may require consideration of such non-equilibrium carrier dynamics.

The presence of multiple switching transitions in individual nanocrystal and film devices also requires further study. The suggested charge order may melt inhomogeneously, with portions of the channel having different switching thresholds. There could also be charge-ordered intermediate states between the insulating regime and the most conducting regime[5]. Again, optical measurements[12] with sufficient spatial resolution could address these possibilities. Through improved metal/magnetite contacts and further study, it should be possible to unravel the precise nature of this non-equilibrium transition, and its relationship to the equilibrium, bulk Verwey transition.

METHODS

Magnetite nanocrystals were prepared using solution-phase decomposition of iron carboxylate salts[19]. The nanocrystals have been characterized by transmission electron microscopy, X-ray diffraction and infrared and Raman spectroscopy, as discussed in Supplementary Information. As-synthesized the nanocrystals are protected by weakly bound oleic acid ligands; these ligands enable the suspension of the nanocrystals in organic solvents, but act as electrically insulating layers that must be largely removed for effective electronic transport measurements.

Two-step electron beam lithography and electron beam evaporation (1 nm Ti, 15 nm Au) were used to pattern closely spaced source and drain electrode pairs onto degenerately n-doped silicon substrates coated with 200 nm of thermally grown SiO_2. Interelectrode gaps (channel lengths) ranged from zero to tens of nanometres, with a 10-μm-wide channel region. Nanocrystals were spin-coated from hexane solutions to form slightly more than one densely packed monolayer of nanocrystals over the channel region. Samples were then baked at 673 K in vacuum for 1 h to remove as much of the oleic acid as possible. In one set of samples, a second layer of particles was added followed by a second round of baking.

The other class of devices is based on epitaxial magnetite films 50 nm thick grown by oxygen-plasma-assisted molecular beam epitaxy on ⟨100⟩ MgO single-crystal substrates. Details of the growth process have been reported elsewhere[20]. Single-step electron beam lithography and electron beam evaporation were used to pattern Au (no Ti adhesion layer) source and drain electrodes defining a channel length ranging from tens to hundreds of nanometres, and a channel width of 20 μm. The interelectrode conduction is dominated by the channel region owing to this geometry. No annealing was carried out following electrode deposition.

Received 24 August 2007; accepted 16 November 2007; published 16 December 2007.

References

1. Mills, A. A. The lodestone: History, physics, and formation. *Ann. Sci.* **61**, 273–319 (2004).
2. Coey, J. M. D. & Chien, C. L. Half-metallic ferromagnetic oxides. *Mater. Res. Soc. Bull.* **28**, 720–724 (2003).
3. Verwey, E. J. W. Electronic conduction in magnetite (Fe_3O_4) and its transition point at low temperatures. *Nature* **144**, 327–328 (1939).
4. Verwey, E. J. W. & Haayman, P. W. Electronic conductivity and transition point of magnetite. *Physica* **8**, 979–987 (1941).
5. Walz, F. The Verwey transition—a topical review. *J. Phys. Condens. Matter* **14**, R285–R340 (2002).
6. Garcıá, J. & Subías, G. The Verwey transition—a new perspective. *J. Phys. Condens. Matter* **16**, R145–R178 (2004).
7. Huang, D. L. *et al.* Charge-orbital ordering and Verwey transition in magnetite measured by resonant soft x-ray scattering. *Phys. Rev. Lett.* **96**, 096401 (2006).
8. Nazarenko, E. *et al.* Resonant x-ray diffraction studies on the charge ordering in magnetite. *Phys. Rev. Lett.* **97**, 056403 (2007).
9. Subías, G. *et al.* Magnetite, a model system for mixed-valence oxides, does not show charge ordering. *Phys. Rev. Lett.* **93**, 156408 (2004).
10. Rozenberg, G. K. *et al.* Origin of the Verwey transition in magnetite. *Phys. Rev. Lett.* **96**, 045705 (2006).
11. Piekarz, P., Parlinksi, K. & Oleś, A. M. Mechanism of the Verwey transition in magnetite. *Phys. Rev. Lett.* **97**, 156402 (2006).
12. Gasparov, L. V. *et al.* Infrared and Raman studies of the Verwey transition in magnetite. *Phys. Rev. B* **62**, 7939–7944 (2000).
13. Imada, M., Fujimori, A. & Tokura, Y. Metal–insulator transitions. *Rev. Mod. Phys.* **70**, 1039–1263 (1998).
14. Coey, M. Condensed-matter physics: Charge-ordering in oxides. *Nature* **430**, 155–157 (2004).
15. Leonov, I., Yaresko, A. N., Antonov, V. N. & Anisimov, V. I. Electronic structure of charge-ordered Fe_3O_4 from calculated optical, magneto-optical Kerr effect, and O *K*-edge x-ray absorption spectra. *Phys. Rev. B* **74**, 165117 (2006).
16. Pinto, H. P. & Elliot, S. D. Mechanism of the Verwey transition in magnetite: Jahn–Teller distortion and charge ordering patterns. *J. Phys. Condens. Matter* **18**, 10427–10436 (2006).
17. Asamitsu, A., Tomioka, Y., Kuwahara, H. & Tokura, Y. Current switching of resistive states in magnetoresistive manganites. *Nature* **388**, 50–52 (1997).
18. Sawa, A., Fujii, T., Kawasaki, M. & Tokura, Y. Hysteretic current–voltage characteristics and resistance switching at a rectifying $Ti/Pr_{0.7}Ca_{0.3}MnO_3$ interface. *Appl. Phys. Lett.* **85**, 4073–4075 (2004).
19. Yu, W. W., Falkner, J. C., Yavuz, C. T. & Colvin, V. L. Synthesis of monodisperse iron oxide nanocrystals by thermal decomposition of iron carboxylate salts. *Chem. Commun.* **2004**, 2306–2307 (2004).
20. Zhou, Y., Jin, X. & Shvets, I. V. Enhancement of the magnetization saturation in magnetite (100) epitaxial films by thermo-chemical treatment. *J. Appl. Phys.* **95**, 7357–7359 (2004).
21. Pérez-Diete, V. *et al.* Thermal decomposition of surfactant coatings on Co and Ni nanocrystals. *Appl. Phys. Lett.* **83**, 5053–5055 (2003).
22. Zeng, H. *et al.* Magnetotransport of magnetite nanoparticle arrays. *Phys. Rev. B* **73**, 020402(R) (2006).
23. Shvets, I. V. *et al.* Long-range charge order on the Fe_3O_4(001) surface. *Phys. Rev. B* **70**, 155406 (2004).
24. Burch, T. *et al.* Switching in magnetite: A thermally driven magnetic phase transition. *Phys. Rev. Lett.* **23**, 1444–1447 (1969).
25. Freud, P. J. & Hed, A. Z. Dynamics of the electric-field-induced conductivity transition in magnetite. *Phys. Rev. Lett.* **23**, 1440–1443 (1969).
26. Duchene, J., Terraillon, M., Pailly, P. & Adam, G. Filamentary conduction in VO_2 coplanar thin-film devices. *Appl. Phys. Lett.* **19**, 115–117 (1971).
27. Gu, Q., Falk, A., Wu, J., Ouyang, L. & Park, H. Current-driven phase oscillation and domain-wall propagation in $W_xV_{1-x}O_2$ nanobeams. *Nano Lett.* **7**, 363–366 (2007).
28. Salazar, A., Oleaga, A., Wiechec, A., Tarnawski, Z. & Kozlowski, A. Thermal diffusivity of $Fe_{3-x}Zn_xO_4$. *IEEE Trans. Magn.* **40**, 2820–2822 (2007).

Acknowledgements

This work was supported by the US Department of Energy grant DE-FG02-06ER46337. D.N. also acknowledges the David and Lucille Packard Foundation and the Research Corporation. V.L.C. acknowledges the NSF Center for Biological and Environmental Nanotechnology (EEC-0647452), Office of Naval Research (N00014-04-1-0003) and the US Environmental Protection Agency Star Program (RD-83253601-0). C.T.Y. acknowledges a Robert A. Welch Foundation (C-1349) graduate fellowship. R.G.S.S. and I.V.S. acknowledge the Science Foundation Ireland grant 06/IN.1/I91. Correspondence and requests for materials should be addressed to D.N.
Supplementary Information accompanies this paper on www.nature.com/naturematerials.

Author contributions

S.L. fabricated and measured the devices in this work and analysed the data. A.F. fabricated devices and carried out X-ray diffraction characterization of the nanocrystal materials. D.N. and S.L. wrote the paper. J.T.M. and C.Y.Z. made the nanocrystals in V.L.C.'s laboratory and V.L.C. contributed expertise in nanomaterials chemistry and characterization. R.G.S.S. and I.V.S. grew the magnetite films and I.V.S. contributed expertise on magnetite physical properties. All authors discussed the results and commented on the manuscript.